

Biomaterials Science

Construction of 3D tumor in vitro models with immune microenvironment exhibited similar tumor properties and biomimetic physiological functionality

Journal:	Biomaterials Science
Manuscript ID	BM-ART-06-2024-000754.R3
Article Type:	Paper
Date Submitted by the Author:	29-Oct-2024
Complete List of Authors:	Jiang, Yuhong; Hunan University Jin, Lijuan; Hunan University Liu, Wenyu; Hunan University Liu, Hui; Hunan University, College of Biology Liu, Xiao; Hunan University, Tan, Zhikai; Hunan University, College of Biology

SCHOLARONE™ Manuscripts

Construction of 3D tumor *in vitro* models with immune microenvironment exhibited similar tumor properties and biomimetic physiological functionality

Yuhong Jiang^{1, 2}, <u>Lijuan Jin</u>³, Wenyu Liu¹, Hui Liu^{1, 2}, Xiao Liu^{3*}, Zhikai Tan^{1, 2, 3*}

Yuhong Jiang and Lijuan Jin have contributed equally to the work.

* Corresponding authors: Dr. Xiao Liu and Dr. Zhikai Tan, Email: 497216514@qq.com; tanzk@hnu.edu.cn;

- College of Biology, Hunan University,
 Changsha, 410082, China
- 2. Institute of Shenzhen, Hunan University Shenzhen, 518000, China
- Greater Bay Area Institute for Innovation, Hunan University,
 Guangzhou, 511300, China

Abstract

Tumors pose a serious threat to people's lives and health, and the complex tumor microenvironment is the biggest obstacle to their treatment. In contrast to the basic protein matrices typically employed in 2D or 3D cell culture systems, decellularized extracellular matrix (dECM) can create complex microenvironments. In this study, a combination of physicochemical methods was established to obtain liver decellularized extracellular matrix scaffolds (dLECMs) as scaffold to provide mechanical support and cell adhesion sites. By co-culturing tumor cells, tumor-associated stromal cells and immune cells, an in vitro 3D tumor model with an biomimetic immune microenvironment were constructed. By utilizing microenvironment data obtained from human liver tumor tissue and refining the double seeding modeling process, 3D in vitro liver tumor-like tissues with a tumor immune microenvironment (TIME) were obtained and designated as reconstructed human liver cancer (RHLC). These tissues demonstrated similar tumor characteristics and exhibited satisfactory physiological functionality. The results of metabolic characterisation and mouse tumorigenicity testing verified that the constructed RHLC significantly increased in vitro drug resistance while also closely mimicking in vivo tissue metabolism. This opens up new possibilities for creating effective in vitro models for screening chemotherapy drugs.

1. Introduction

Cancer is a leading cause of human mortality and a major impediment to increasing life expectancy [1]. Human tumors are highly complex, and their significant heterogeneity is considered as the primary barrier to developing effective, patient-specific treatment approaches [2,3]. Different tumor phenotypes dynamically evolve during disease progression and clinical therapy. Therefore, deciphering tumor heterogeneity and establishing cancer research models capable of systematically defining and simulating tumor heterogeneity are of utmost importance and difficulty.

Currently, the traditional models for cancer research in laboratories are animal models and 2D culture models-cell line models. Although cell lines are easy to manipulate, it is challenging to simulate the intricate relationships that exist between cells and the tumor microenvironment [4–8]. Animal models are an effective tool for understanding pathogenesis and therapeutic approaches [9]. However, animal models tend to replace exogenous tumor stromal cells and immune cells with their own cells, limiting their predictability as tumor models [10,11]. Therefore, 3D bioengineered tumor models have been established in this study to better simulate the intricate internal environment of tumors, serving as a bridge between animal and human experiments[12].

It is still a challenge to establish a biomimetic 3D bioengineered tumor models. For conventional 3D hydrogel materials, the key bioactive factors needed for tissue engineering are absent, while decellularized extracellular matrix (dECM) scaffolds have been demonstrated to contain a wide variety of extracellular matrix components and a multitude of growth factors [13,14]. Therefore, extracellular matrix (ECM) has been used to create a range of 3D bioengineered tumor in vitro models. Besides, natural liver ECM is one type of ECMs that can create a complex and biomimetic microenvironment [15,16]. It retains part of the morphology, ECM components, and ultrastructure of organs to support hepatocyte viability and function [17,18]. Furthermore, dLECMs is widely recognized as supporting hepatocellular carcinoma

cell line culture and is considered a promising naturally derived biomaterial for *in vitro* hepatocyte culture [19-21]. Therefore, in this study, dLECMs were utilized as the foundational material for establishing 3D tumor models. Besides, the traditional single method of dECM preparation is ineffective[22]; therefore, this study employed a combination of physical and chemical methods supplemented with the use of nuclease for the effective preparation of dLECMs.

The development of tumors is influenced by the surrounding environment, in which various cell types exist in a dynamic milieu that regulates tumor growth, invasion, and spread. Currently, the disparity between 3D tumor tissues and actual tumor tissues is primarily due to the absence of their unique microenvironment. For example, the absence of tumor-related endothelial cells can lead to tissue hypoxia, resulting in suboptimal 3D tumor construction [23]. Most solid tumors are composed of stromal cells, including cancer-associated fibroblasts (CAF), immune cells, tumour endothelial cells (TEC), adipocytes, ECM proteins, and soluble molecules such as cytokines, chemokines, or growth factors. These elements collectively constitute the distinct tumor microenvironment (TME) [24-26]. Numerous methods exist for simulating the TME, among which multicellular co-culture was proved to be a valuable approach [27,28]. Moreover, common 3D models usually lack an immune system, which is an incomplete model for the determination of anticancer drugs [29]. Immunotherapy has become a viable new treatment option for cancer in recent years. Since the therapeutic benefit is less than anticipated in a significant percentage of patients, researchers tend to examine the immune response against tumors in greater detail and to develop more suitable algorithms for forecasting each patient's response to therapy. New approaches to tissue engineering can help produce humanized stromabased models in vitro [30]. Therefore, in this study, activated stromal cells CAF, TEC, immune cells JURKAT, and dLECMs were used as non-tumor components to establish RHLC by multi-cell co-culture with HepG2. Metabolic characterization and nude mouse tumorigenicity testing are utilized to value the RHLC, and the RHLC exhibits with possesses robust metabolic functionality and resistance to chemotherapy might be a potential model for preclinical drug screening.

2. Materials and Methods

2.1. Preparation of dLECMs

Fresh pig liver was acquired from a slaughterhouse, cut into 5 mm³ cubes, placed in an ultra-low-temperature refrigerator overnight. The tissue sample was rinsed three times with deionized water for 5 minutes each time, and this process was repeated three times. The tissue samples was then placed in an ion washing buffer (containing 1% (v/v) Triton X-100 (Sigma) and 0.5% (w/v) SDS (Sinopharm, China), as well as Phosphate Buffered Saline (PBS) solution with an appropriate amount of antibiotics and stirred. After two days, the waste solution was filtered out using a funnel, and the tissue was rinsed three times with sterile PBS for 5 minutes each time. This process was repeated multiple times until the tissue became transparent. Finally, the samples was washed with nuclease (70 U/ml nuclease, 50 mM/L Tris-C1) (Yesen, China) for 24 hours. The rinsed transparent tissue samples were washed several times with sterile PBS to remove residual Triton X-100 and SDS. The samples were then immersed in 75% medical alcohol for two hours, exposed to UV radiation for 1 hour, and stored at -20°C.

2.2. dLECMs Characterization

To validate the decellularization process of pork liver, tissue sections were subjected to component analysis using H&E staining kit (Solarbio, China) and Masson staining kit (Solarbio, China). Fresh liver tissue and dLECMs were paraffin-embedded for histological staining and observed under bright-field microscopy using an inverted fluorescence microscope IX73 (Research-grade) (Olympus). The morphology of the decellularized tissue and cell adhesion after cell seeding were examined by scanning electron microscopy (SEM). The dLECMs and cell-seeded scaffolds were coated with Pt and observed using SEM (EM-30/X-ACT, COXEM) at a voltage of 10 kV. The major DNA components were analyzed using DAPI (Yesen, China) and the DNeasy kit.

2.3. Cell Compatibility and Phenotypic Assessment

The human liver cancer cells (HepG2), human umbilical vein endothelial cells (HUVEC), human embryonic lung fibroblasts (HELF), and human T lymphocyte leukemia cells (JURKAT) used in the experiments were sourced from the Chinese Academy of Sciences Cell Repository. JURKAT cells, were cultured in 1640 medium (10% FBS + 1% PS) (Gibco), while other cells were cultured in DMEM medium (10% Fetal Bovine Serum (FBS)+ 1% Penicillin-Streptomycin Solution(PS)) (Gibco). For the culture of 3D cells, dLECMs were first adhered to culture dishes. After the scaffolds adhered, culture medium was added and allowed to infiltrate for 2 hours. Subsequently, the culture medium was removed, and an appropriate number of cells were seeded in the incubator for 4-6 hours. Once cell adhesion to the scaffold was observed under a microscope, fresh culture medium was added to initiate 3D culture, and the medium was changed when it turned yellow. The viability of HepG2 cells in 3D cultures after 3 days was measured using a Calcein-AM/Propidium Iodide (PI) Live-Dead staining kit (Solarbio, China). The control group was the culture dish group (2D). To evaluate the impact of 24-hour culture in 2D and 3D conditions on the phenotype of HepG2 cells, staining was performed using Anti-Vinculin antibody (Proteintech, China) and Anti-Ki67 antibody (Proteintech, China). For assessing the impact on HELF cell phenotype, staining was done using Anti-MMP2 antibody (Proteintech, China). Cells were resuspended in 500 µL PBS (1 X 10⁵ cells/tube) and analyzed using a flow cytometer (CytoFLEX, Beckman Coulter).

2.4. Activation of Stromal Cells

When HepG2 cell density reached 80%, the culture medium was replaced, and incubation continued for another 24 hours to collect the supernatant after centrifugation, which was used as conditioned medium (CM) (referred to as HepG2 CM). Normal stromal cells (HELF and HUVEC) were seeded in regular culture medium, and after reaching confluency, they were switched to HepG2 CM culture medium (100%) and incubated for an additional 48 hours. Subsequently, they were respectively activated into cancer-associated fibroblasts (CAF) and tumor-associated endothelial cells (TEC).

To assess the degree of stromal cell activation, immunofluorescence was performed. Anti-α-Smooth Muscle Actin antibody (Anti-α-SMA, Proteintech, China) and DAPI (Yesen, China) were used for co-staining of HELF and CAF. Anti-CD144 antibody (Proteintech, China), TRITC Phalloidin (Yesen, China), and DAPI (Yesen, China) were used for co-staining of HUVEC and TEC. Observations were made under an inverted fluorescence microscope IX73 (Research Grade) (Olympus). Real-time PCR was also conducted to evaluate gene expression. After 48 hours of culture in 6 cm culture dishes, RNA extraction was carried out using RNAiso Plus (Takara) and chloroform (Sinopharm, China). Reverse transcription of RNA into cDNA was performed using the inNova Uscript II All in One First-strand cDNA Synthesis SuperMix (Innovagene) (Vazyme). Tag SYBR Green qPCR Premix (With ROX) (Innovagene) was used for qPCR with β-actin as an internal reference. The expression of genes including Fibroblast activation protein-α (FAP), Fibroblast-specific protein 1 (FSP1), Collagen I, Transforming Growth Factor-β (TGF-β) for CAF, and Tumor endothelial marker 1 (TEM1), Tumor endothelial marker 8 (TEM8), Vascular Endothelial Growth Factor (VEGF), and Biglycan for TEC was analyzed (Table 1).

Table 1. Primer Sequences

gene	Forward primer sequences	Reverse primer sequence
β-actin	TGGCACCCAGCACAATGAA	CTAAGTCATAGTCCGCCTAGA
		AGCA
FAP	ACGGCTTATCACCTGATCGG	AATTGGACGAGGAAGCTCAT
		TT
TGF-β1	ACTGCAAGTGGACATCAACG	TGCGGAAGTCAATGTACAGC
Collagen I	ATCAAGGTCTACTGCAACAT	CAGGATCGGAACCTTCGCT
FSP1	GATGAGCAACTTGGACAGC	CTGGGCTGCTTATCTGGGAAG
	AA	
Biglycan	AGGAGGCGGTCCATAAGAA	AGGGTTGAAAGGCTGGAAAT
	T	

VEGF	TTGCCTTGCTGCTCTACCTCC	GATGGCAGTAGCTGCGCTGA
	A	TA
TEM 8	CGGATTGCGGACAGTAAGG	GCCAGAACCACCAGAGGAG
TEM 1	TCGAGTGTTATTGTAGCGAG	AGGTGGGCTCCGGGTAGGGT
	GGACATG	AT

2.5. Screening of Human Tumor Tissue Information

Paraffin sections of human liver cancer tissue samples were obtained from Xiangya Hospital and subjected to immunohistochemical staining. After antigen retrieval, they were incubated with primary antibodies, including alpha-fetoprotein (Anti-AFP) and Anti-CD45 Antibodies (Proteintech, China), for 24 hours. Subsequently, they were incubated at room temperature with HRP-labeled secondary antibodies for 40 minutes, followed by incubation in DAB working solution for 5 minutes. After staining with hematoxylin, counterstaining, dehydration, and drying, observations were made under an inverted fluorescence microscope IX73 (Research Grade) (Olympus).

2.6. Construction of Tumor Tissues

Four groups with consistent cell numbers were employed to establish the tumor microtissue model. Control Group: A mixture of HepG2, HUVEC, and HELF cells in a 5:1:1 ratio was evenly seeded onto dLECMs. Activation Group: A mixture of HepG2, TEC, and CAF cells in a 5:1:1 ratio was evenly seeded onto dLECMs. Double Seeding Group: After two days of cell culture in the Activation Group, a second seeding with the same ratios was performed, maintaining the same cell numbers as the first seeding. Immune Environment Group: A mixture of HepG2, TEC, CAF, and JURKAT cells in a 30:6:6:5 ratio was evenly seeded onto dLECMs, as depicted in the schematic diagram of tumor tissue construction (Graphical abstract). Following cell culture for 3, 7, 15, and 30 days, live cell staining was conducted using the calcein-AM/propidium iodide (PI) live-dead staining reagent (Solarbio, China), and observations were made under a laser confocal microscope (Olympus).

2.7. Physiological Function Characterization

2.7.1. Metabolic Capacity Assessment

To assess the metabolic changes of *in vitro* tumor tissues, we collected cell culture supernatants after culturing the tumor tissues *in vitro* for 1, 3, 5, and 7 days. Glucose content was determined following the instructions of a glucose assay kit (Solarbio, China), and lactate (LD) content was measured using an LD assay kit (Nanjing Jiangcheng Bioengineering Institute, China). We followed the kit instructions to set up the groups, and after the reaction with the reagents, the absorbance at the corresponding wavelengths (505 nm for glucose and 570 nm for lactate) was measured using a Nanodrop 2000 (Thermo SCIENTIFIC).

2.7.2. Drug Resistance Capability

The dosage of two chemotherapeutic agents was set as follows: 5-Fluorouracil (5Fu) at $25 \mu M$ and Doxorubicin (Dox) at $10 \mu M$. Prior to drug administration, it is imperative to observe the cultured cells, initiating drug treatment only when the cells have reached their optimal growth state. Following the addition of drugs to the culture medium, gently agitate the culture dish to ensure uniform drug distribution. Subsequently, continue the cultivation in an incubator for an additional 24 hours. To characterize the drug resistance of *in vitro* tumor tissues after treatment with two anti-cancer chemotherapy drugs, DOX and 5-FU, we used a CCK8 assay kit (Solarbio, China) to assess cell viability. The groups were set up according to the kit instructions, and after the reaction with the reagents, the absorbance at 450 nm was measured using a Nanodrop 2000 (Thermo SCIENTIFIC).

2.7.3. Evaluation of Cell Viability

To further investigate the metabolic differences between immune cells, 2D culture, and 3D culture, as well as the drug resistance of tumor tissues, flow cytometry analysis was conducted. To assess cell viability, we employed PI dye (Calcein-AM/Propidium iodide-PI Live-Dead Staining Kit, Solarbio, China). Apoptosis experiments used the Annexin V apoptosis assay kit (Thermo Fisher), and analysis was performed using a

CytoFLEX flow cytometer (Beckman Coulter).

2.8. Tumorigenicity Assessment of Tumor Microtissues

All animal procedures were performed in accordance with the Guidelines for Care and Use of Laboratory Animals of Hunan University and approved by the Animal Ethics Committee of Hunan University (Permit No. HNUBIO202101009). Five-week-old athymic nude mice were randomly divided into five groups. Group A consisted of HepG2 cells cultured in 2D. Group B included HepG2, TEC, and CAF co-cultured in 2D. Group C involved co-culture of HepG2, TEC, CAF, and JURKAT cells in 2D. Group D included HepG2, TEC, and CAF co-cultured in a 3D environment. Group E comprised HepG2, TEC, CAF, and JURKAT cells co-cultured in a 3D environment. The number of cells was consistent among all groups. In the 3D group, cells were coimplanted with dLECMs under the skin of the nude mice. To ensure consistency, the cell-seeded scaffold was placed under the skin of the mice immediately after removing it from the culture dish. Each group of mice was housed separately, and their body weight was measured every three days. A caliper was used to measure the length and width of the tumors. Tumor volume was estimated based on the formula, where "L" represents the measured length of the tumor, and "W" represents the measured width of the tumor.

Tumor volume (mm³) =
$$\frac{4}{3}\pi \left(\frac{W}{2}\right)^2 \left(\frac{L}{2}\right) = 0.52W^2L$$

2.9. Statistical Analysis

Each group included a minimum of three parallel data points, and inter-group comparisons were performed using a t-test, and the comparisons between three groups or more groups were conducted by one way analysis of variance (ANOVA). Graphical analysis and plotting were conducted using Prism 8. Statistical significance was considered when p < 0.05. The significance levels between groups were represented as **** (p < 0.0001), *** (p < 0.001), ** (p < 0.001), and * (p < 0.05).

3. Results

3.1. Preparation and Characterization of dLECMs

To obtain fiber-rich dLECMs as a scaffold for RHLC. Based on previous methods [31], the preparation of dLECMs was optimized and the brief process was illustrated (Figure 1A). The dLECMs displayed a porous network structure (Figure 1B), as seen in SEM, revealing a fibrous mesh-like structure conducive to cell adhesion (Figure 1C). The success of tissue construction is closely related to the residual components of the dLECMs. Therefore, we performed DAPI staining, HE staining, and Masson staining on the dLECMs (Figure 1D-F). The results indicated that after the decellularization process cellular components were removed effectively while the ECM components were retained. DAPI staining (Figure 1D) and H&E staining (Figure 1E) confirmed that after decellularization, nearly all intact nuclei were removed, and a significant amount of cellular debris was eliminated. Masson trichrome staining confirmed that the remaining ECM components were predominantly collagen fibers (Figure 1F), and most of the elastin fibers were removed after decellularization (Figure 1G), and collagen fibers were abundant (Figure 1H). Subsequent DNA content analysis showed that the ECM group had less than 50 ng/mg, meeting the standard of double-stranded DNA content below 50 ng per milligram of ECM [32]. This further demonstrates that the nucleus component was mostly extracted during decellularization (Figure 1I). These results showed that the cellular components in liver tissue were effectively removed while a large number of collagen fibers were retained, and dLECMs were successfully prepared, making them ideal scaffolds for the construction of three-dimensional RHLC.

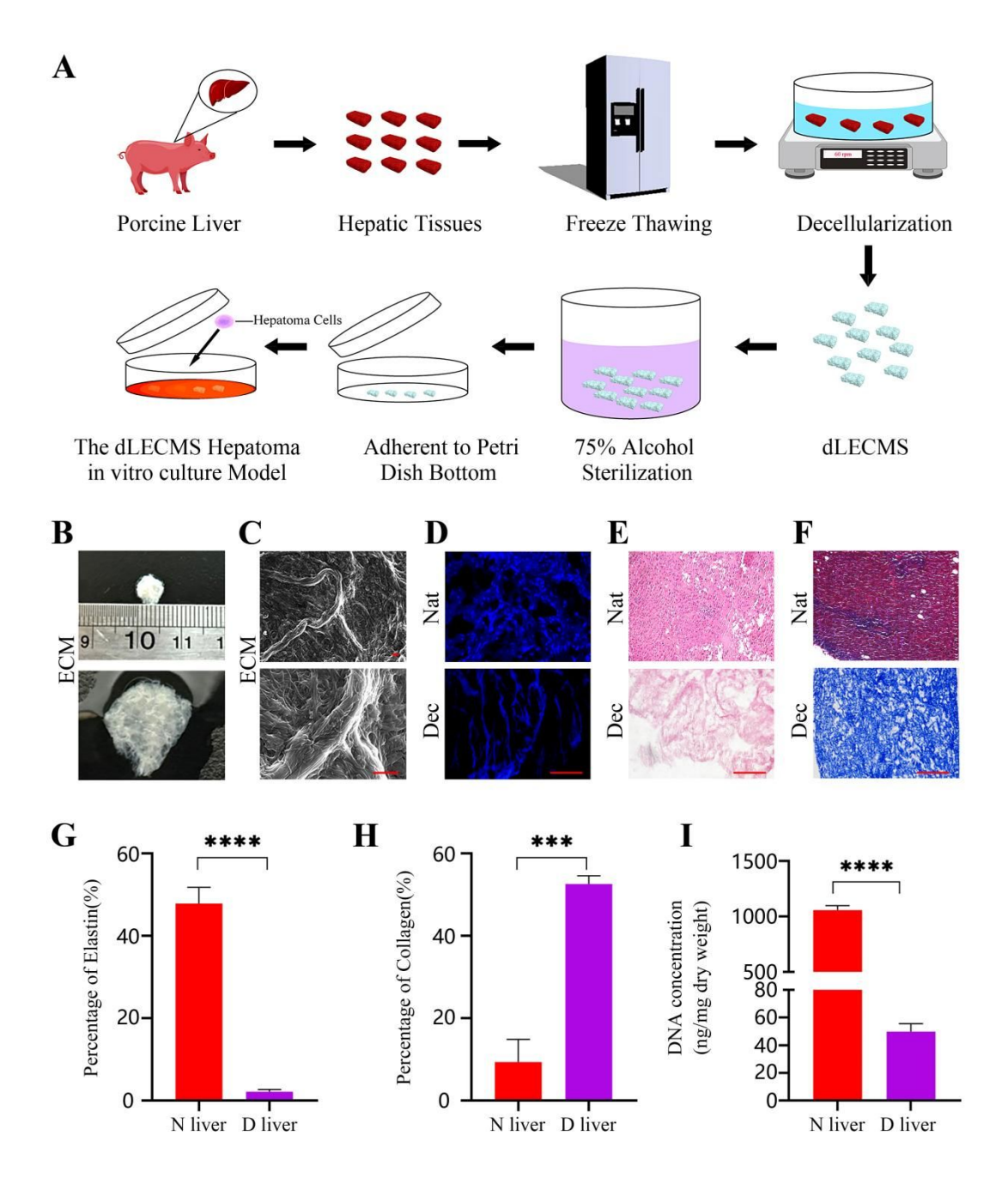


Figure 1. Preparation, Identification, and Characterization of dLECMs. (A) Schematic diagram of dLECMs preparation. (B) Physical diagram of dLECMs. Dimensions of dLECMs (top), and morphology of dLECMs (bottom). (C) Scanning electron microscope (SEM) images of dLECMs. dLECMs for low magnification (top), and dLECMs for high magnification (bottom). Scale bar = 1 μ m. (D) DAPI staining results of liver tissue and dLECMs. (E) H&E staining results of liver tissue and dLECMs. (F) Masson staining results of liver tissue and dLECMs. (D-F) Nat: native liver tissue, Dec:

decellularized liver tissue. Scale bar = $100 \mu m.(G)$ Quantification of elastic fibers. (H) Quantification of collagen.(I) DNA content analysis. (G-I) N liver: native liver tissue, D liver: decellularized liver tissue.

3.2. In vitro Cell Compatibility and Cell Phenotype Regulation

To determine the cytotoxicity and regulatory role of dLECMs as RHLC scaffolds. Live/dead staining results demonstrate that after HepG2 cell cultured for 3 days, there is no significant difference in the number of live and dead cells compared to 2D culture. The cell state appears to be saturated, and no pathological changes are observed (Figure 2A and Figure 2B). This suggests that dLECMs are non-toxic to cells and exhibit good biocompatibility. Flow cytometry results showed that, compared to 2D culture, tumor cells on dLECMs exhibit higher levels of Vinculin (Figure 2C) and Ki67 (Figure 2D) expression, indicating that adhesion and proliferation capabilities of tumor cells were enhanced in the dLECMs. Besides, matrix metalloproteinases (MMPs) are important mediators of fibroblasts in extracellular matrix remodeling, and dLECMs induce fibroblasts to express more MMP2 (Figure 2E). These results suggest that dLECMs have good cytocompatibility, which is conducive to the regulation of tumor cell adhesion, proliferation and extracellular matrix remodeling, and can provide a good growth environment for cells.

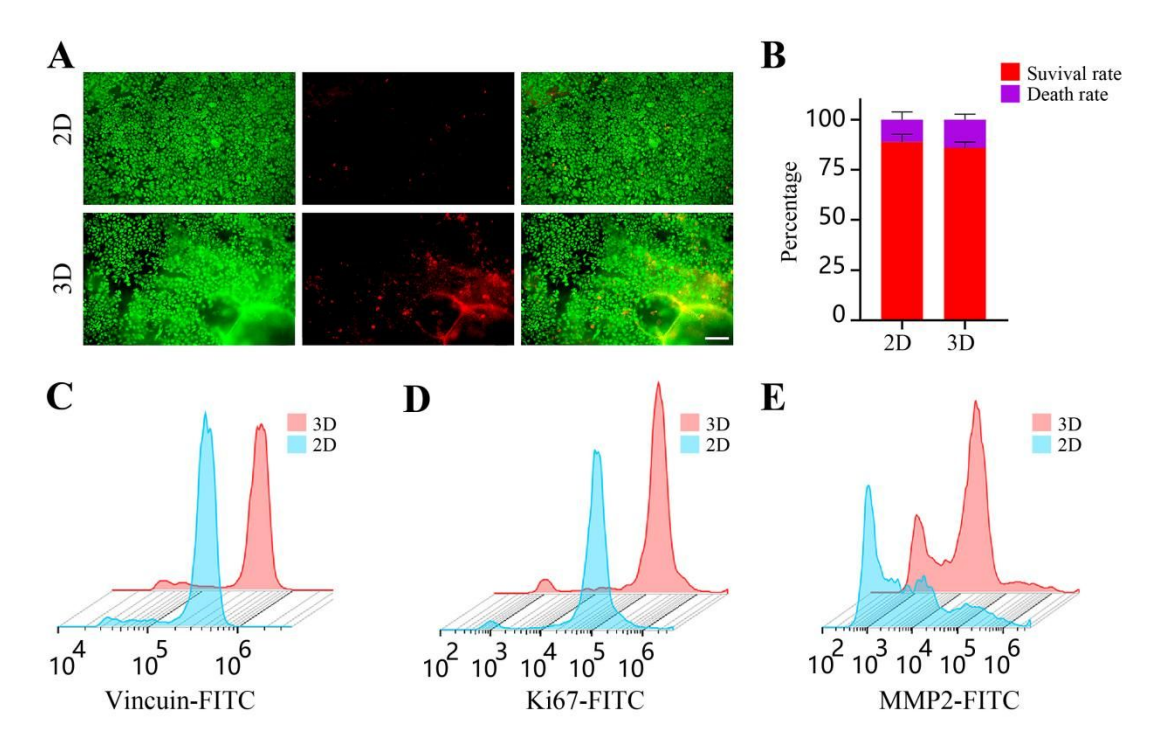


Figure 2. Toxicity Assessment and Functional Characterization of dLECMs. (A) Live cells (green), dead cells (red), scale bar = $200 \mu m$. (B) Quantification of live and dead cells in the image from (A) using Image J. (C) Expression of Vinculin in HepG2 cells. (D) Expression of Ki67 in HepG2 cells.(E) Expression of MMP2 in CAF (Cancer-Associated Fibroblasts). (C-E) Flow cytometry results comparing 2D culture (blue) and 3D culture (dLECMs) (red).

3.3. Activation of Tumor-Associated Stromal Cells

The formation of tumors is accompanied by changes in the surrounding stroma, where tumor-associated stromal cells create a suitable tumor microenvironment for tumor growth. To obtain tumor-associated stromal cells required for RHLC construction, we activated stromal cells to become tumor-associated stromal cells. After stimulating HELF with conditioned medium from tumor cells for 48 hours, immunofluorescence results showed an upregulation of α -SMA expression in CAF, accompanied by a change in cell morphology from elliptical shape to spindle-shape (Figure 3A), which resembles the appearance of CAF. Fluorescence quantitative PCR experiments were conducted for FAP, FSP, Collagen I and TGF- β . The results revealed a significant upregulation in expression in CAF

compared to HELF (Figure 3C). Upon stimulation of HUVEC with conditioned medium from tumor cells for 48 hours, immunofluorescence results demonstrated an upregulation of CD144 expression in TEC (Figure 3B), accompanied by a change in cell morphology from rounded to dendritic (Figure 3D), which indicate a more mature vascular structure of TEC. To further validate the activation of HUVEC, we examined the expression of TEM1, TEM8, VEGF, and Biglycan. The results revealed an upregulation in expression in TEC compared to HUVEC (Figure 3E) which consistent with previous reports[33]. These results indicated that HELF was activated to CAF and HUVEC was activated to TEC. Successful acquisition of tumor-associated stromal cells could provide a tumor microenvironment for RHLC construction.

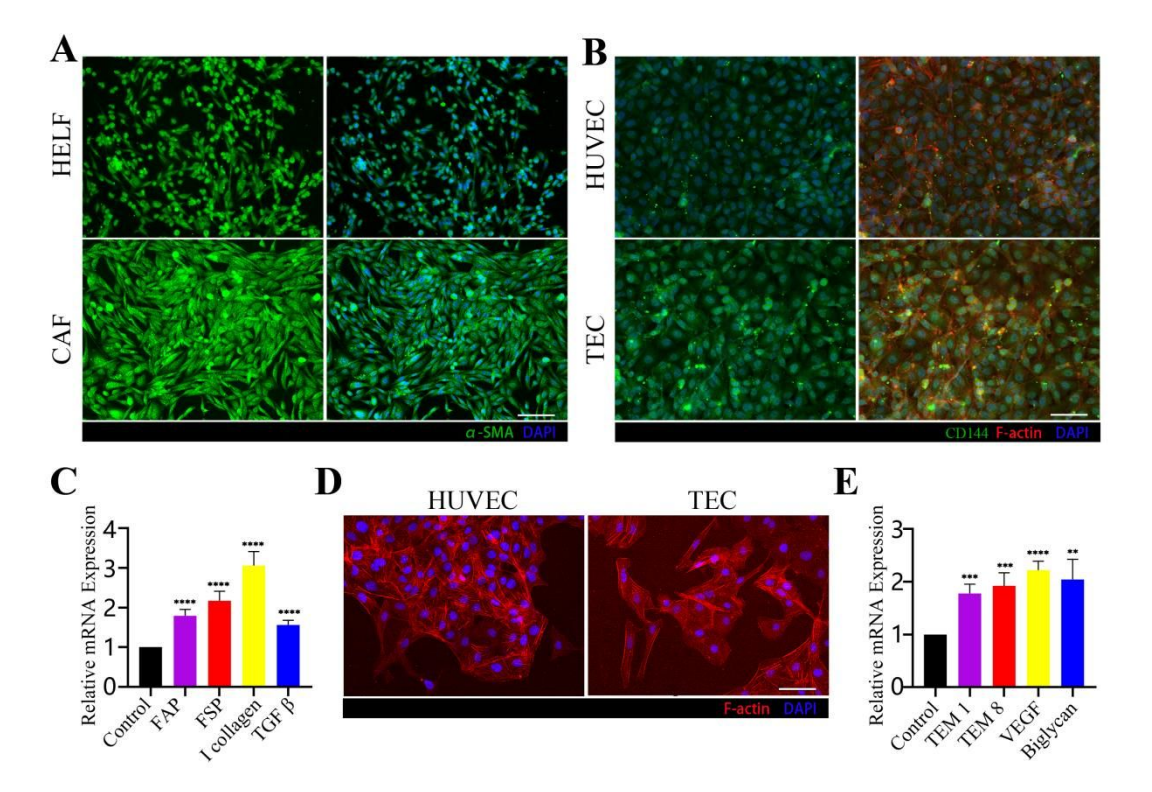


Figure 3. The Activation of Tumor-Associated Stromal Cells Was Assessed 48 Hours After Stimulation. (A) Immunofluorescence staining images of α-SMA (green) in normal fibroblasts (HELF) and tumor-associated fibroblasts (CAF). (B) Immunofluorescence staining images of specific protein CD144 (green) in normal endothelial cells (HUVEC) and tumor-associated endothelial cells (TEC). (C) Gene expression analysis of CAF markers FAP, FSP, collagen I, and TGF β. (D)

Immunofluorescence staining images of cytoskeleton (red) in HUVEC and TEC. Scale bar = 200 μ m. (E) Gene expression analysis of TEC markers TEM1, TEM8, VEGF, and Biglycan (****, p<0.0001; ***, p<0.001; **, p<0.01; n=5).

3.4. Construction of RHLC

To determine the cell ratio and inoculation method required to construct the RHLC. In this study, the cell ratio in the tumor tissue model was determined based on human tumor tissue samples and previous laboratory modeling experience [33]. Immunohistochemical staining images and quantification results of AFP and CD45 showed the cell ratio of hepatic cells and immune cells was around 6:1 in human liver tumor tissue (Figure 4A-C). Combining previous experiences in modeling colorectal cancer [33], the cell ratios for in vitro co-culture were established as HepG2:CAF:TEC:JURKAT = 30:6:6:5. Several modeling approaches were compared and optimized for the construction of tumor microtissues (Figure 4D), the surviving microtissues were adhered to the dLECMs (Figure 4E). Live cell staining results indicated that when unactivated stromal cells were co-cultured with tumor cells, microtissues survived at 3 days but died off completely at 7 days. However, when activated stromal cells were co-cultured with tumor cells, microtissues survived after 7 days. The process of cell aggregation into tissue is time-consuming and requires a significant amount of cells to generate an "aggregation effect." When stromal cells and tumor cells were co-cultured for 2 days and then re-seeded, small amounts of microtissues survived at 15 days. The immune microenvironment is associated with tumor progression, as immune cells secrete various cytokines that promote tumor growth. Many microtissues persisted even after 30 days when tumor cells were cocultured with immune cells and activated stromal cells with second-seed, and distributed tumor aggregates were seen on dLECMs with tubulointerstitial structures generation (Figure 4F). Besides, the H&E staining also verified the existence of cell aggregates resembling tissue structures (Figure 4G). These results indicate that the cell ratio required for RHLC construction was HepG2:CAF:TEC:JURKAT = 30:6:6:5, and the inoculation method was that HepG2, TEC, CAF, and JURKAT were co-cultured in dLECMs, and a second inoculation was done on the next day, which greatly prolonged the lifespan of the constructed RHLC, allowing it to mimic tumor tissue formation and exhibit vascular-like structures. Hence, the construction of RHLC was established following this protocol and culture condition in this article.

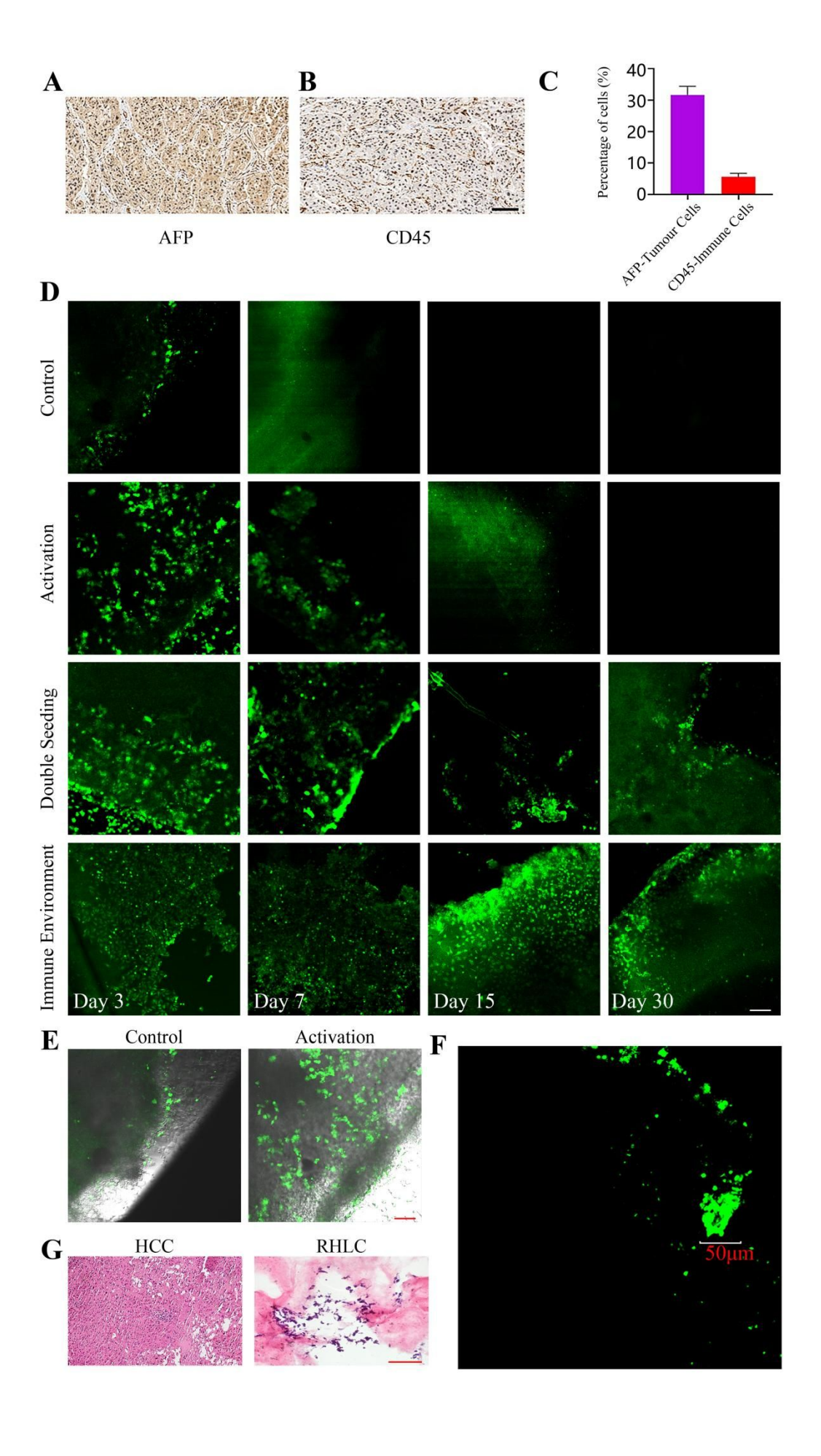


Figure 4. Human Liver Tumor Tissue Cell And Information Screening Construction of *in vitro* Tumor Tissues with an Immune Microenvironment. (A) Immunohistochemical staining image of the liver cancer marker AFP. (B) Immunohistochemical staining image of the immune cell marker CD45. (C) Quantification of (A) and (B), with an AFP:CD45 ratio of 6:1. Scale bar = 100 μm.

(D) Live cell staining results of tumor tissues. Control group: Co-culture of HepG2, HUVEC, and HELF on dLECMs for 3, 7 days. Activation group: Co-culture of HepG2, TEC, and CAF on dLECMs for 3, 7, 15 days. Double Seeding group: Two days of cell culture in the Activation group, followed by reseeding in the same proportions for 3, 7, 15, 30 days. Immune Environment group: HepG2, TEC, CAF, and JURKAT were inoculated into dLECMs for co-culture, and the second inoculation was performed on the next day to continue the culture for 3, 7, 15, and 30 days. Scale bar = $200 \mu m$. (E) Merged bright-field images of dLECMs and live cell staining. Control group: HepG2, HUVEC, and HELF were inoculated into dLECMs for 3 days (left). Activation group: Co-culture of HepG2, TEC, and CAF on dLECMs for 3 days (right). Scale bar = 200 μm. (F) Live cell staining images of microtissues on dLECMs. Immune Environment group: HepG2, TEC, CAF, and JURKAT were inoculated into dLECMs for co-culture, and the second inoculation was performed on the next day to continue the culture for 30 days. Scale bar = 50 μm. (G) H&E staining images comparing human tumor tissue(hepatocellular carcinoma, HCC)(left) with in vitro constructed 3D tumor-like tissue with TIME (reconstructed human liver cancer,RHLC) (right). Scale bar = 100 μm.

3.5. Metabolic Function Assessment of RHLC

To explore the tumor properties of RHLC, its metabolic capacity including glucose and lactate levels and cell viability were examined. Four groups were chosen to determine glucose and lactate concentrations in the culture medium,: 2D-HepG2-CAF-TEC (2D-Immunodeficiency), dLECMs (3D)-HepG2-CAF-TEC (3D-Immunodeficiency), 2D-

HepG2-CAF-TEC-JURKAT (2D-Immune), and dLECMs (3D)-HepG2-CAF-TEC-JURKAT (3D-Immune, RHLC). The glucose detection results (Figure 5A) indicate that the rate of consumption in 3D is faster than that of 2D. The glucose concentration in 3D drops below 0.1 mmol/L after 5 days, whereas it remains around 0.1 mmol/L in 2D even after 7 days. Moreover, 3D-Immune (RHLC) exhibits a faster glucose consumption rate compared to 3D-Immunodeficiency. Lactate detection results (Figure 5B) indicate that more lactate were generated in 3D than that of 2D. Moreover, 3D-Immune (RHLC) demonstrates the highest efficiency in lactate production. Simultaneously, flow cytometry results demonstrate that 3D-Immune (RHLC) exhibits higher cellular viability compared to 2D-Immune (Figure 5C). 2D and 3D - immune CM culture of immune cells (JURKAT) was used to explore the effect of different dimensions of conditioned medium (CM) on immune cells. Immune cells (JURKAT) CM culture of 2D and 3D-Immunodeficient cells was used to explore the effect of immune cell conditioned medium (CM) on immunodeficient cells of different dimensions. Flow cytometry revealed that the cellular activity of immune cells showed similar tendency in 2D and 3D CM (Figure 5D). However, the immune cells CM improved the cell activity of 3D-Immunodeficiency. As shown in Figure 5E, the activity of 3D-Immunodeficiency was significantly enhanced when cultured with JURKAT CM. This improvement may be attributed to soluble molecules secreted by immune cells, creating an immunosuppressive microenvironment that protects tumor cells from destruction and promotes tumor cells proliferation. In summary, the introduction of the immune microenvironment improves the growth conditions for tumor cells, making tumor cells metabolism more vigorous. These data suggest that RHLC, consist of 3D liver decellularized extracellular matrix scaffolds with multi-cell co-culture and immune microenvironment, have similar tumor properties and are the most metabolically active compared to the other groups, since it exhibit the fastest rate of glucose consumption and the fastest rate of lactate production as well as the strongest cell viability.

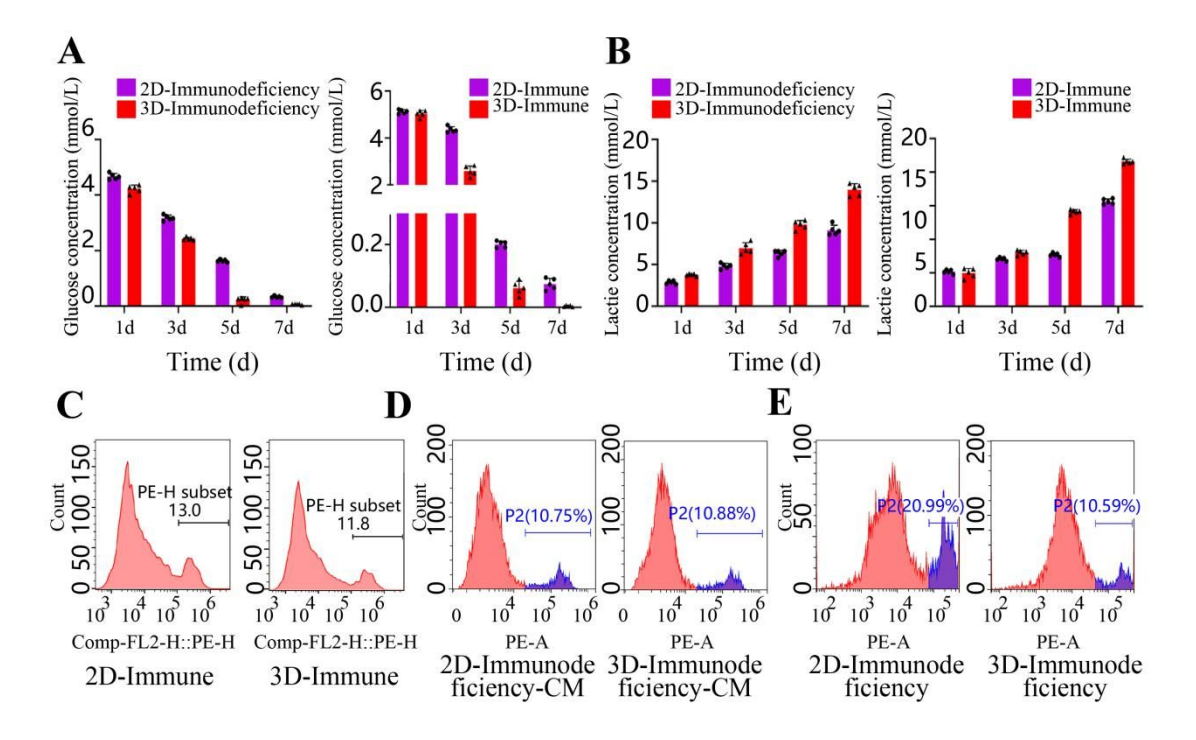


Figure 5. Metabolic Function Assessment of RHLC. (A) Glucose (505 nm) and (B) lactate (570 nm) concentrations in the culture medium of tumor microtissues cultured for 1, 3, 5, and 7 days. Flow cytometry with propidium iodide (PI) staining was employed to assess cellular activity in 2D-Immune and 3D-Immune (Figure C). The impact of 2D-Immunodeficiency and 3D-Immunodeficiency CM on the cellular activity of immune cells (JURKAT) was examined (Figure D). Additionally, the influence of immune cells (JURKAT) CM on the cellular activity of 2D-Immunodeficiency and 3D-Immunodeficiency was investigated (Figure E).

3.6. In vivo Tumorigenicity and in vitro Drug Resistance Analysis

To determine the biomimetic physiological function of RHLC, its tumorigenicity and drug resistance were analyzed. For a more comprehensive analysis, five groups were set: 2D-HepG2, 2D-HepG2-CAF-TEC (2D-Immunodeficiency), 2D-HepG2-CAF-TEC-JURKAT (2D-Immune), dLECMs (3D)-HepG2-CAF-TEC (3D-Immunodeficiency), and dLECMs (3D)-HepG2-CAF-TEC-JURKAT (3D-Immune, RHLC). The results of Subcutaneous tumor tissue development in nude mice after 30 days (Figure 6B) demonstrated that 3D tumor tissues exhibited cystic morphology with

compact structure, and the darker red color indicated greater stromal vascularization, in comparison to tumor tissues without dLECMs. In all groups, 2D-HepG2 tumor volume was the smallest and 2D-Immune tumor volume was greater than 2D-Immunodeficiency. Tumor volume results (Figure 6C) indicate that multicellular seeding promotes tumor tissue growth. Additionally, the incorporation of dLECM significantly enhances malignant tumor growth, leading to rapid and aggressive expansion. 3D-immune and 3D-Immunodeficiency tumors have similar growth trends. Interestingly, in the 2D setting, the inclusion of immune cells plays a critical role in promoting tumor growth. However, in the 3D environment, the impact of immune cells on tumor growth is less pronounced. This may be attributed to altered cell-cell interactions and the barrier function of the extracellular matrix in the 3D environment. There were no significant differences in the mice's body weight between the groups (Figure 6D). Although 3D-Immune and 3D-Immunodeficiency have similar tumors growth rates, 3D-Immune (RHLC) has a more significant cell viability compared with 3D-Immunodeficiency after treatment of chemotherapeutic medicines DOX and 5-FU (Figure 6E). Multi-cell co-culture increases cell viability compared to single-cell culture. Experiments on apoptosis further shown that, in contrast to single-cell and 2D co-cultures, 3D tumor microtissues showed higher levels of drug resistance after chemotherapy, and that 3D-Immune (RHLC) showed lower levels of apoptosis (Figure 6F). These results suggest that RHLC has a better bionic physiological function, since RHLC resembles the in vivo tumor microenvironment and showed excellent in vivo tumorigenicity and drug resistance.

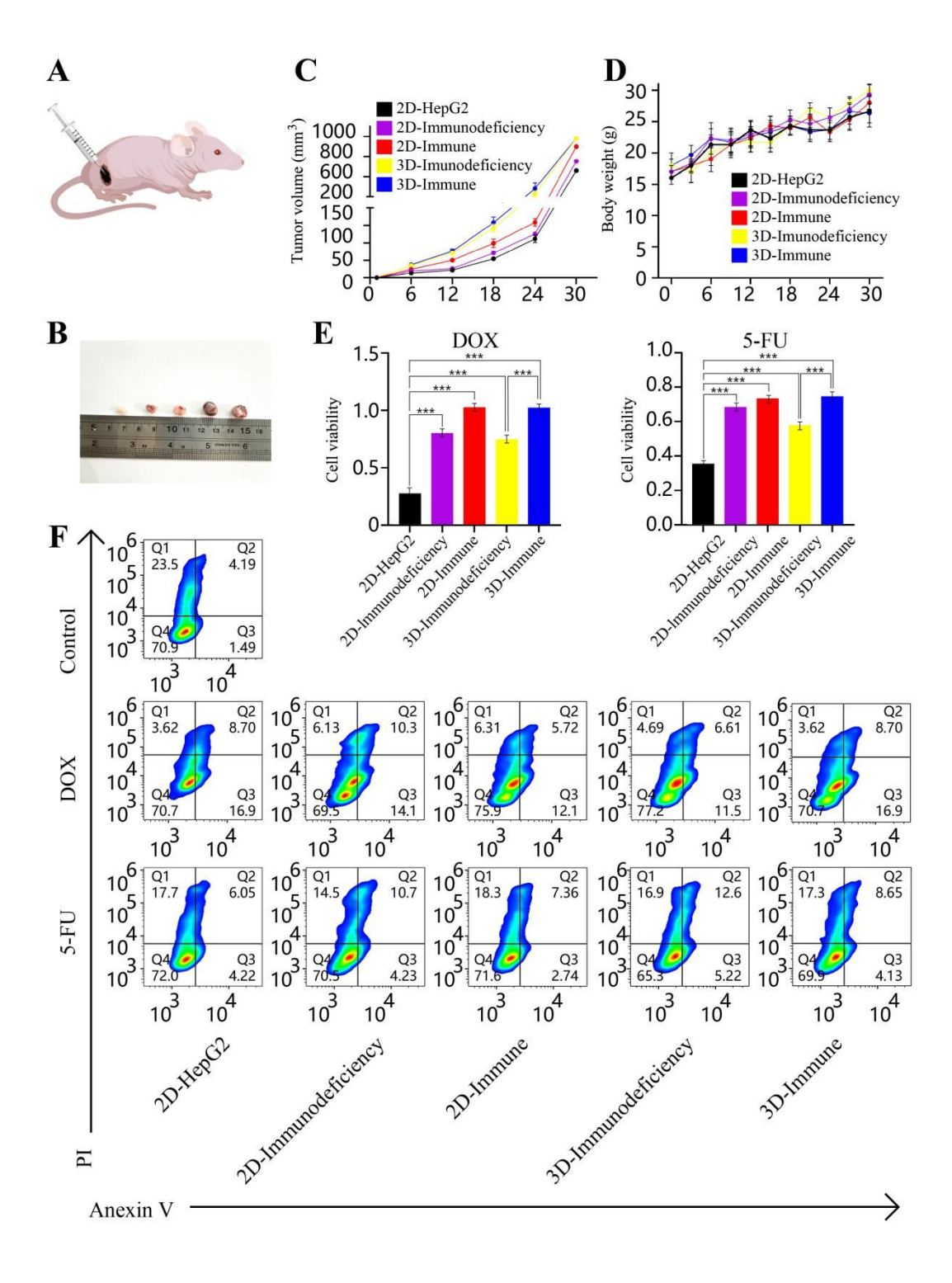


Figure 6. Tumorigenicity and Drug Resistance of Microtumor Tissues. (A) Subcutaneous tumor implantation model in mice. (B) Images of tumors harvested from nude mice in different groups after 30 days of subcutaneous tumorigenesis. (C) Tumor volume changes at various time points in each group. (D) Changes in body weight of the mice in different groups. (E) Changes in cell viability after treatment with

chemotherapy drugs DOX and 5-FU (***, p<0.001; n=3). (F) Results of apoptosis flow cytometry analysis with chemotherapy drugs DOX and 5-FU.

4. Discussion

Scaffold, as one of the core elements in tissue engineering, serves the purpose of providing mechanical support for tissue growth and creating a microenvironment conducive to tissue growth[34]. Traditional dECM preparation may not be capable of complete cell elimination effectively[22]. In this study, a combination of physical and chemical methods was employed for decellularization, complemented by the use of nucleases to remove surplus immunogenic materials. Results from HE staining and DAPI staining demonstrate the effectiveness of this method in thoroughly removing cellular components. Quantitative DNA analysis indicates that the enzymatic treatment method successfully eliminates immunogenic materials. dECM comprises a variety of components, and collagen as well as growth factors are important[35]. Masson staining results reveal that dLECMs contains collagen, elastin and a small quantity of elastic fibers. Besides, researches have validated that collagen can provide mechanical support and promote cell adhesion[36]. And scanning electron microscopy was used to observe the dLECMs, revealing a mesh-like porous structure with a significant matrix presence, might favor cell adhesion within dLECMs.

The dLECMs, as a natural biomaterial, could also mediate cellular phenotype. Compared to 2D culture, HepG2 cells in dLECMs express higher levels of Vinculin and Ki67. This suggests that dLECMs can induce cell proliferation and adhesion, thereby influencing cell phenotype changes. In the context of tumor modeling, stromal cells are indispensable, and the essential mediator of stromal remodeling by fibroblasts is matrix metalloproteinase 2 (MMP2). MMP2 holds significant physiological importance in tumor tissues[37]. Experimental validation indicates that dLECMs can promote the enhanced expression of MMP2 in stromal cells, which showed the positive role of dLECMs in inducing stromal remodeling phenotypes.

The tumor microenvironment (TME) plays a crucial role in altering cancer progression and treatment responses. A significant barrier to the advancement of cancer therapies is the discrepancy between the TME in tumor models and that of patients [38]. The tremendous heterogeneity of cell types within the TME is crucial for treatment response. 3D organotypic culture of cancer types offers advantages in recapitulating the original tumor histology and mutational characteristics, facilitating long-term propagation for experimental research[39]. To model the complex tumor microenvironment, many researchers have established research platforms through multicellular co-cultures [40-42]. However, it may not fully encompass the multicellular composition of the TME [43-45]. In addition to tumor cells, research suggests that tumors are composed of multiple components such as stromal cells and immune cells that contributed to their tumoral heterogeneity[46], Therefore, in this article, we established 3D in vitro liver tumour-like tissues with a tumour immune microenvironment (TIME) . Besides, the phenotype of normal stromal cells differs from that of stromal cells within tumors. Therefore, in this study, tumor-associated stromal cells were induced by exposing stromal cells to the CM containing factors secreted by tumor cells. A comparison between activated and non-activated stromal cells revealed that the former enhanced the adhesion of co-cultured cells to the dLECMs. The development of tumors is closely linked to an immunosuppressive microenvironment. The unique immunosuppressive microenvironment of tumor tissues can protect tumor cells from destruction and create a favorable microenvironment for tumor cell growth. Since primary immune cells are difficult to obtain and expensive to culture, immune cell lines were chosen. And T lymphocyte leukemia cells have been selected for their high expression of CD3, low levels of CD4, and possession of immune cell functions [47,48].

The establishment of tumor models requires consideration of various factors, and in a multicellular co-culture system, the seeding ratio of individual cells has a significant impact on tumor modeling. With the goal of creating biomimetic RHLC, cell seeding ratio data followed cellular information from hepatic tumor tissues. Based on successful

laboratory experiences in the construction of 3D colorectal cancer tumors, a seeding ratio of HepG2:CAF:TEC:JURKAT=30:6:6:1 [33] was adopted for the construction of the tumor tissue. In addition, the number of cells seeded also profoundly affects the efficiency of tumor tissue construction. Thus, secondary seeding was employed. Experimental results indicated that secondary seeding enabled the survival of tumor tissue for over 15 days, and the introduction of immune cells formed a pronounced immunosuppressive microenvironment, significantly extending the lifespan of the tumor tissue. Through in vitro metabolic function experiments and drug resistance assays, it was demonstrated that RHLC exhibits robust metabolic functionality and drug heterogeneity. Subsequent in vivo tumorigenesis experiments in nude mice further validated that the RHLC exhibits robust physiological functions, including metabolic activity and drug resistance. In general, potential new targets for immunotherapy may be discovered via the obtained RHLC, and RHLC could also be used as a in vitro experiments model for investigating drug delivery particles or nanoscale theranostics[49], rendering it a valuable platform for drug screening and development. In the current study, the obtained RHLC were proved to be robust metabolic activity and high drug resistance, and a comprehensive assessment of cellular properties such as proliferation, adhesion, and metabolism has been conducted, but further researches still need on revealing the operation mechanism of the obtained co-cultured system, such as cytoskeletal arrangement, paracrine and cell migration of the different cells which will provide crucial supplementary information for understanding the tumor microenvironment. Via analyzing the arrangement of the cytoskeleton, insights can be gained into how tumor cells adapt to and reshape their structure in a 3D microenvironment, and cell migration is a critical step in tumor metastasis, investigating the migratory and paracrine behavior of cells within 3D scaffolds can reveal the dynamic interactions between different cell types within the tumor microenvironment. Besides the hinder might be how to distinguish or label the different cells since so many kinds of cells were in the system, the indirect co-culture model and

staining specific cell markers simultaneously might be utilized in follow-up studies.

5. Conclusion

In this study, a facile and effective approach was employed to fabricate a 3D scaffold suitable for tumour remodelling (dLECMs). The dLECMs exhibit excellent biocompatibility, promoting cell growth and effectively regulate cell phenotypes. The activation of stromal cells into tumor-associated stromal cells was successfully achieved. Through multicellular co-culture involving secondary seeding of tumor cells, tumor-associated fibroblasts, tumor-associated endothelial cells and immune cells, a 3D *in vitro* liver tumor-like tissues with a tumor immune microenvironment (RHLC) was successfully constructed. The RHLC demonstrates robust metabolic activity and high drug resistance, making it a valuable preclinical model for drug screening. These findings offer novel insights for the further development of 3D *in vitro* tumor models.

Conflicts of interest

The authors declare that they have no competing interests.

Data Availability Statemen

All relevant data are available and have been included in this paper

Acknowledgements

This study was financially supported by the Research and Development Plan of Key Fields in Hunan Province (No. 2022SK2027), Natural Science Foundation of Guangdong Province (No. 2023A1515011463), High-end Foreign Experts Recruitment Plan of China (No. G2023160019L), Shanghai Key Laboratory of Peripheral Nerve and Microsurgery (20DZ2270200-202402), NHC Key Laboratory of Hand Reconstruction (Fudan University), Institute of Hand Surgery, Shanghai.

References

- [1] Bray F, Laversanne M, Weiderpass E, Soerjomataram I. The ever-increasing importance of cancer as a leading cause of premature death worldwide. Cancer. 2021 Aug 15;127(16):3029-3030.
- [2] Bedard PL, Hansen AR, Ratain MJ, Siu LL. Tumour heterogeneity in the clinic. Nature. 2013 Sep 19;501(7467):355-64.
- [3] Dagogo-Jack I, Shaw AT. Tumour heterogeneity and resistance to cancer therapies. Nat Rev Clin Oncol. 2018 Feb;15(2):81-94.
- [4] Chatterjee S, Naidu GS, Hazan-Halevy I, Grobe H, Ezra A, Sharma P, Goldsmith M, Ramishetti S, Sprinzak D, Zaidel-Bar R, Peer D. Therapeutic gene silencing of CKAP5 leads to lethality in genetically unstable cancer cells. Sci Adv. 2023 Apr 5;9(14):eade4800.
- [5] Hanahan D, Weinberg RA. Hallmarks of cancer: the next generation. Cell. 2011 Mar 4;144(5):646-74.
- [6] Smalley KS, Lioni M, Herlyn M. Life isn't flat: taking cancer biology to the next dimension. *in vitro* Cell Dev Biol Anim. 2006 Sep-Oct;42(8-9):242-7.
- [7] Gillet JP, Varma S, Gottesman MM. The clinical relevance of cancer cell lines. J Natl Cancer Inst. 2013 Apr 3;105(7):452-8.
- [8] Katt ME, Placone AL, Wong AD, Xu ZS, Searson PC. *in vitro* Tumor Models: Advantages, Disadvantages, Variables, and Selecting the Right Platform. Front Bioeng Biotechnol. 2016 Feb 12;4:12.
- [9] Yan K, Gao H, Liu X, Zhao Z, Gao B, Zhang L. Establishment and identification of an animal model of long-term exercise-induced fatigue. Front Endocrinol (Lausanne). 2022 Aug 26;13:915937.
- [10] Malaney P, Nicosia SV, Davé V. One mouse, one patient paradigm: New avatars of personalized cancer therapy. Cancer Lett. 2014 Mar 1;344(1):1-12.
- [11] Frederico SC, Zhang X, Hu B, Kohanbash G. Pre-clinical models for evaluating glioma targeted immunotherapies. Front Immunol. 2023 Jan 9;13:1092399.
- [12] Sharma A, Sances S, Workman MJ, Svendsen CN. Multi-lineage Human iPSC-

- Derived Platforms for Disease Modeling and Drug Discovery. Cell Stem Cell. 2020 Mar 5;26(3):309-329.
- [13] Wang R, He X, Chen Z, Su S, Bai J, Liu H, Zhou F. A nanoparticle reinforced microporous methacrylated silk fibroin hydrogel to promote bone regeneration. Biomater Sci. 2024 Mar 8.
- [14] Almalla A, Elomaa L, Bechtella L, Daneshgar A, Yavvari P, Mahfouz Z, Tang P, Koksch B, Sauer I, Pagel K, Hillebrandt KH, Weinhart M. Papain-Based Solubilization of Decellularized Extracellular Matrix for the Preparation of Bioactive, Thermosensitive Pregels. Biomacromolecules. 2023 Dec 11;24(12):5620-5637.
- [15] Ferreira LP, Gaspar VM, Mano JF. Decellularized Extracellular Matrix for Bioengineering Physiomimetic 3D *in vitro* Tumor Models. Trends Biotechnol. 2020 Dec;38(12):1397-1414.
- [16] Ma X, Yu C, Wang P, Xu W, Wan X, Lai CSE, Liu J, Koroleva-Maharajh A, Chen S. Rapid 3D bioprinting of decellularized extracellular matrix with regionally varied mechanical properties and biomimetic microarchitecture. Biomaterials. 2018 Dec;185:310-321.
- [17] Baptista PM, Siddiqui MM, Lozier G, Rodriguez SR, Atala A, Soker S. The use of whole organ decellularization for the generation of a vascularized liver organoid. Hepatology. 2011 Feb;53(2):604-17.
- [18] Ott HC, Matthiesen TS, Goh SK, Black LD, Kren SM, Netoff TI, Taylor DA. Perfusion-decellularized matrix: using nature's platform to engineer a bioartificial heart. Nat Med. 2008 Feb;14(2):213-21.
- [19] Wang Y, Cui C-B, Yamauchi M, Miguez P, Roach M, Malavarca R, Costello MJ, Cardinale V, Wauthier E, Barbier C, Gerber DA, Alvaro D, Reid LM, Lineage restriction of human hepatic stem cells to mature fates is made efficient by tissue-specific biomatrix scaffolds, Hepatology 53 (2011) 293–305.
- [20] Park K-M, Hussein KH, Hong S-H, Ahn C, Yang S-R, Park S-M, Kweon O-K, Kim B-M, Woo H-M, Decellularized liver extracellular matrix as promising tools for

- transplantable bioengineered liver promotes hepatic lineage commitments of induced pluripotent stem cells, Tissue Eng. Part A 22 (2016) 449–460.
- [21] Cheng Y, Wang Y, Kang YZ, Hu PY, Gao Y, Pan MX, *in vitro* culture of tumourderived hepatocytes in decellularised whole-liver biological scaffolds, Digestion 87 (2013) 189–195.
- [22] Zhang X, Chen X, Hong H, Hu R, Liu J, Liu C. Decellularized extracellular matrix scaffolds: Recent trends and emerging strategies in tissue engineering. Bioact Mater. 2021 Sep 23;10:15-31.
- [23] Choi NW, Cabodi M, Held B, Gleghorn JP, Bonassar LJ, Stroock AD. Microfluidic scaffolds for tissue engineering. Nat Mater. 2007 Nov;6(11):908-15.
- [24] Hanahan D, Weinberg RA. Hallmarks of cancer: the next generation. Cell. 2011 Mar 4;144(5):646-74.
- [25] Labani-Motlagh A, Ashja-Mahdavi M, Loskog A. The Tumor Microenvironment: A Milieu Hindering and Obstructing Antitumor Immune Responses. Front Immunol. 2020 May 15;11:940.
- [26] Cox TR. The matrix in cancer. Nat Rev Cancer. 2021 Apr;21(4):217-238.
- [27] Öhlund D, Handly-Santana A, Biffi G, Elyada E, Almeida AS, Ponz-Sarvise M, Corbo V, Oni TE, Hearn SA, Lee EJ, Chio II, Hwang CI, Tiriac H, Baker LA, Engle DD, Feig C, Kultti A, Egeblad M, Fearon DT, Crawford JM, Clevers H, Park Y, Tuveson DA. Distinct populations of inflammatory fibroblasts and myofibroblasts in pancreatic cancer. J Exp Med. 2017 Mar 6;214(3):579-596.
- [28] Biffi G, Oni TE, Spielman B, Hao Y, Elyada E, Park Y, Preall J, Tuveson DA. IL1-Induced JAK/STAT Signaling Is Antagonized by TGFβ to Shape CAF Heterogeneity in Pancreatic Ductal Adenocarcinoma. Cancer Discov. 2019 Feb;9(2):282-301.
- [29] Shukla P, Yeleswarapu S, Heinrich MA, Prakash J, Pati F. Mimicking tumor microenvironment by 3D bioprinting: 3D cancer modeling. Biofabrication. 2022 May 31;14(3).

- [30] Vitale C, Marzagalli M, Scaglione S, Dondero A, Bottino C, Castriconi R. Tumor Microenvironment and Hydrogel-Based 3D Cancer Models for In Vitro Testing Immunotherapies. Cancers (Basel). 2022 Feb 17;14(4):1013.
- [31]Sabetkish S, Kajbafzadeh AM, Sabetkish N, Khorramirouz R, Akbarzadeh A, Seyedian SL, Pasalar P, Orangian S, Beigi RS, Aryan Z, Akbari H, Tavangar SM. Whole-organ tissue engineering: decellularization and recellularization of three-dimensional matrix liver scaffolds. J Biomed Mater Res A. 2015 Apr;103(4):1498-508. [32] Qiao S, Peijie T, Nan J. Crosslinking strategies of decellularized extracellular matrix in tissue regeneration. J Biomed Mater Res A. 2024 May;112(5):640-671.
- [33] Chen H, Cheng Y, Wang X, Wang J, Shi X, Li X, Tan W, Tan Z. 3D printed *in vitro* tumor tissue model of colorectal cancer. Theranostics. 2020 Oct 26;10(26):12127-12143.
- [34] Habanjar O, Diab-Assaf M, Caldefie-Chezet F, Delort L. 3D Cell Culture Systems: Tumor Application, Advantages, and Disadvantages. Int J Mol Sci. 2021 Nov 11;22(22):12200.
- [35] Won JY, Lee MH, Kim MJ, Min KH, Ahn G, Han JS, Jin S, Yun WS, Shim JH. A potential dermal substitute using decellularized dermis extracellular matrix derived bio-ink. Artif Cells Nanomed Biotechnol. 2019 Dec;47(1):644-649.
- [36] Amirrah IN, Lokanathan Y, Zulkiflee I, Wee MFMR, Motta A, Fauzi MB. A Comprehensive Review on Collagen Type I Development of Biomaterials for Tissue Engineering: From Biosynthesis to Bioscaffold. Biomedicines. 2022 Sep 16;10(9):2307. [37]Théret N, Musso O, L'Helgoualc'h A, Campion JP, Clément B. Differential expression and origin of membrane-type 1 and 2 matrix metalloproteinases (MT-MMPs) in association with MMP2 activation in injured human livers. Am J Pathol. 1998 Sep;153(3):945-54.
- [38]Lv J, Du X, Wang M, Su J, Wei Y, Xu C. Construction of tumor organoids and their application to cancer research and therapy. Theranostics. 2024 Jan 12;14(3):1101-1125.

- [39] Haykal MM, Nahmias C, Varon C, Martin OCB. Organotypic Modeling of the Tumor Landscape. Front Cell Dev Biol. 2020 Nov 24;8:606039.
- [40] Malacrida B, Nichols S, Maniati E, Jones R, Delanie-Smith R, Roozitalab R, Tyler EJ, Thomas M, Boot G, Mackerodt J, Lockley M, Knight MM, Balkwill FR, Pearce OMT. A human multi-cellular model shows how platelets drive production of diseased extracellular matrix and tissue invasion. iScience. 2021 May 29;24(6):102676.
- [41] Taubenberger AV, Bray LJ, Haller B, Shaposhnykov A, Binner M, Freudenberg U, Guck J, Werner C. 3D extracellular matrix interactions modulate tumour cell growth, invasion and angiogenesis in engineered tumour microenvironments. Acta Biomater. 2016 May;36:73-85.
- [42] Sameni M, Anbalagan A, Olive MB, Moin K, Mattingly RR, Sloane BF. MAME models for 4D live-cell imaging of tumor: microenvironment interactions that impact malignant progression. J Vis Exp. 2012 Feb 17;(60):3661.
- [43]Weeber F, van de Wetering M, Hoogstraat M, Dijkstra KK, Krijgsman O, Kuilman T, Gadellaa-van Hooijdonk CG, van der Velden DL, Peeper DS, Cuppen EP, Vries RG, Clevers H, Voest EE. Preserved genetic diversity in organoids cultured from biopsies of human colorectal cancer metastases. Proc Natl Acad Sci U S A. 2015 Oct 27;112(43):13308-11.
- [44] van de Wetering M, Francies HE, Francis JM, Bounova G, Iorio F, Pronk A, van Houdt W, van Gorp J, Taylor-Weiner A, Kester L, McLaren-Douglas A, Blokker J, Jaksani S, Bartfeld S, Volckman R, van Sluis P, Li VS, Seepo S, Sekhar Pedamallu C, Cibulskis K, Carter SL, McKenna A, Lawrence MS, Lichtenstein L, Stewart C, Koster J, Versteeg R, van Oudenaarden A, Saez-Rodriguez J, Vries RG, Getz G, Wessels L, Stratton MR, McDermott U, Meyerson M, Garnett MJ, Clevers H. Prospective derivation of a living organoid biobank of colorectal cancer patients. Cell. 2015 May 7;161(4):933-45.
- [45] Clevers H. Modeling Development and Disease with Organoids. Cell. 2016 Jun 16;165(7):1586-1597.

- [46]Lavallee E, Sfakianos JP, Mulholland DJ. Tumor Heterogeneity and Consequences for Bladder Cancer Treatment. Cancers (Basel). 2021 Oct 22;13(21):5297.
- [47] Roose JP, Diehn M, Tomlinson MG, Lin J, Alizadeh AA, Botstein D, Brown PO, Weiss A. T cell receptor-independent basal signaling via Erk and Abl kinases suppresses RAG gene expression. PLoS Biol. 2003 Nov;1(2):E53.
- [48] Borst J, Ahrends T, Bąbała N, Melief CJM, Kastenmüller W. CD4+ T cell help in cancer immunology and immunotherapy. Nat Rev Immunol. 2018 Oct;18(10):635-647.
- [49] Wu Z, Zhang H, Yan J, Wei Y, Su J. Engineered biomembrane-derived nanoparticles for nanoscale theranostics. Theranostics. 2023 Jan 1;13(1):20-39.

Data Availability Statemen

All relevant data are available and have been included in this paper